RESULTS FROM NOMAD

Alberto Marchionni
INFN, Sezione di Firenze
Largo E. Fermi 2, I-50125 Firenze, Italy

Representing the NOMAD Collaboration

ABSTRACT

The NOMAD experiment at CERN is conducting a search for $\nu_\mu \to \nu_\tau$ oscillations, for neutrino squared mass differences larger than about 1 eV^2. The ν_τ is searched for via its charged current interactions, where the τ lepton is identified through its decay products by means of kinematical criteria. Present results show no evidence for oscillations and allow us to set the 90% confidence level limit of $\sin^2 2\theta_{\mu\tau} < 1.2 \times 10^{-3}$ at large Δm^2.

1 Introduction

In the Standard Model of electroweak interactions,[1] the existence of three different generations in the quark sector with corresponding generations in the leptonic sector is a solid experimental fact, but whose deep reason is still unexplained. The presence of mixing between the different generations in the quark sector has been known since a long time and it is presently described by the Cabibbo-Kobayashi-Maskawa matrix (see Ref. 2 for a review). In the leptonic sector, the conservation of a lepton family number has been assumed. Searches for processes of the type $\mu \to e\gamma$ have provided only upper limits so far.[2]

Neutrino oscillations,[3] first proposed by B. Pontecorvo in the late '50s, might be a more sensitive way to search for lepton family number violation. If neutrinos are massive, it is likely that the mass eigenstates are different from the weak interaction eigenstates, which could then be written as a linear superposition of the mass eigenstates. In a simplified two-generation approach, if $\mid \nu_1\rangle$ and $\mid \nu_2\rangle$ are the mass eigenstates with masses m_1 and m_2, respectively, and $\mid \nu_\alpha\rangle$ and $\mid \nu_\beta\rangle$ are the flavor eigenstates, then:

$$\begin{pmatrix} \nu_\alpha \\ \nu_\beta \end{pmatrix} = \begin{pmatrix} \cos\theta & \sin\theta \\ -\sin\theta & \cos\theta \end{pmatrix} \begin{pmatrix} \nu_1 \\ \nu_2 \end{pmatrix},$$

where θ is the "mixing angle." The probability P that a neutrino of energy E, originally in a state $\mid \nu_\alpha\rangle$, is in a state $\mid \nu_\beta\rangle$ after a distance L from the point where it was generated, is given by:

$$P(\nu_\alpha \to \nu_\beta) = \sin^2(2\theta)\sin^2(1.27\Delta m^2 L/E),$$

where $\Delta m^2 = \mid m_1^2 - m_2^2 \mid \mathrm{eV}^2$ and L/E is expressed in km/GeV.

In order that the oscillation probability P be different from zero, it is necessary that $\theta \neq 0$ and $\Delta m^2 \neq 0$. The existence of the phenomenon of neutrino oscillations is thus directly connected to the question of whether neutrinos are massive and indeed it provides a way to measure the Δm^2 parameter.

Recent experimental results[4] from atmospheric and solar neutrino experiments, and from the LSND experiment give some indications for the existence of neutrino oscillations. The interpretation of these results in a complete three-generation approach is still far from clear, in particular for what concerns the Δm^2's involved in the process.

The NOMAD experiment[5,6] at CERN, together with its companion experiment CHORUS,[7] is investigating the region $\Delta m^2 > 1$ eV^2. The original motivation of NOMAD is the search for a cosmologically relevant neutrino mass.[8] Big Bang relic neutrinos, if there is at least one mass eigenstate with $m > 1$ eV, would play an important role in the evolution of the universe.

The NOMAD experiment, which has been carried out on the CERN wide-band neutrino beam, is investigating both $\nu_\mu \to \nu_\tau$ and $\nu_\mu \to \nu_e$ oscillation channels. It is an appearance experiment where the identification of ν_τ charged current (CC) interactions relies purely on kinematical criteria.

A description of the experimental method and a discussion of present results will be given for the $\nu_\mu \to \nu_\tau$ oscillation channel, which has been the primary motivation of the experiment. The search for $\nu_\mu \to \nu_e$ oscillations from the available data sample is not completed yet. The result depends critically on the knowledge of the systematic error on the flux and spectrum of the electron neutrino component in the beam. An effort to precisely determine the neutrino beam composition is currently underway.

2 The Experimental Apparatus

The NOMAD detector is installed on the neutrino beam of the West Area Neutrino Facility (WANF) at CERN. After an overview of the neutrino beam, a description of the detector is given.

2.1 The Neutrino Beam

The WANF wide-band neutrino beam[9] (see Fig. 1) is produced from the decays of secondary π and K mesons originated in the interactions of 450 GeV/c protons from the SPS on a Be target. In order to obtain a beam composed mainly of neutrinos, with a small contamination of antineutrinos, positively charged particles from the target

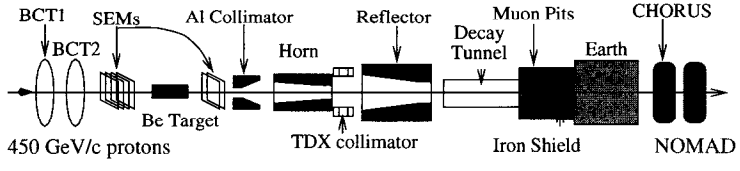

Fig. 1. Schematic layout of the West Area Neutrino Facility at CERN (not drawn to scale).

are focused by a pair of coaxial magnetic lenses (the horn and the reflector), while negative particles are defocused. The mesons are allowed to decay in a 290 m long vacuum tunnel, which is followed by a shield of iron and earth for the absorption of the undecayed hadrons.

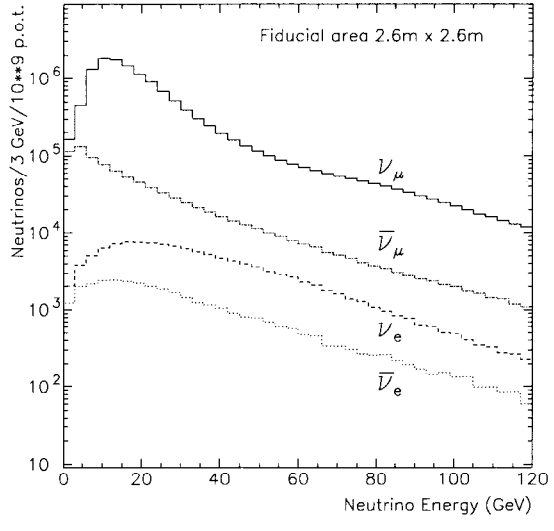

Fig. 2. Energy spectra of the different components of the neutrino beam at the NOMAD position.

The NOMAD detector is installed at 835 m from the Be target, at a mean distance of 620 m from the hadron decay position. The resulting neutrino spectra from π and K decays are shown in Fig. 2 at the position of the NOMAD detector, integrated over an area of 2.6×2.6 m^2. Table 1 summarizes mean energies and relative abundances of the different components of the neutrino beam and of the resulting interactions in the detector.

The beam is mainly composed of muon neutrinos, with an electron neutrino contamination of the order of 1%. Interactions of the "wrong sign" components $\overline{\nu}_\mu$ and $\overline{\nu}_e$ are present at the level of about 2% and 0.2% of the ν_μ interactions, respectively. The presence of prompt ν_τ in the beam, coming from charmed meson D_s decays, has been estimated[10] to be negligible. They amount to about 5×10^{-6} of the ν_μ interactions, thus resulting in much less than one event detectable in NOMAD.

Table 1. Summary of mean energies and relative abundances of the different components of the neutrino beam and of the resulting interactions.

	Flux		Interactions	
Neutrino	$\langle E_\nu \rangle$ (GeV)	Rel. Abund.	$\langle E_\nu \rangle$ (GeV)	Rel. Abund.
ν_μ	23.6	1.0	44.1	1.0
$\overline{\nu}_\mu$	18.4	0.055	40.6	0.021
ν_e	37.5	0.009	56.6	0.015
$\overline{\nu}_e$	30.3	0.0025	50.7	0.0016
ν_τ	~ 35			$\simeq 5 \times 10^{-6}$

The average value of the L/E (traveled distance over energy) distribution of ν_μ neutrinos interacting in NOMAD is about 1.5×10^{-2} km/GeV. Thus the maximum Δm^2 sensitivity is at about 90 eV^2, making the experiment sensitive to the cosmologically relevant mass range.

2.2 The Detector

The NOMAD detector[6] has been designed to detect ν_τ CC interactions through different τ decay channels by means of kinematical criteria which require a detailed reconstruction of the event. Thus a detector is needed which is capable of a precise measurement of charged particles, a good identification of electrons and muons, an accurate measurement of electromagnetic showers and of neutral hadron detection.

The NOMAD detector (see Fig. 3) is located in a large dipole magnet which provides a field of 0.4 T over a volume of $7.5 \times 3.5 \times 3.5$ m^3. The magnetic field direction is horizontal and orthogonal to the beam line.

A set of 44 drift chambers constitute at the same time the target material for neutrino interactions and the tracking device of the experiment. Materials of low atomic number have been employed for the construction of the chambers in order to minimize multiple scattering of charged particles and photon conversions. Chamber panels made of Aramid fibers in a honeycomb structure sandwiched by two Kevlar-epoxy resin skins provide the necessary mechanical rigidity and flatness over a large surface area of 3×3 m^2. The total fiducial mass of the target amounts to 2.7 tons over a volume of

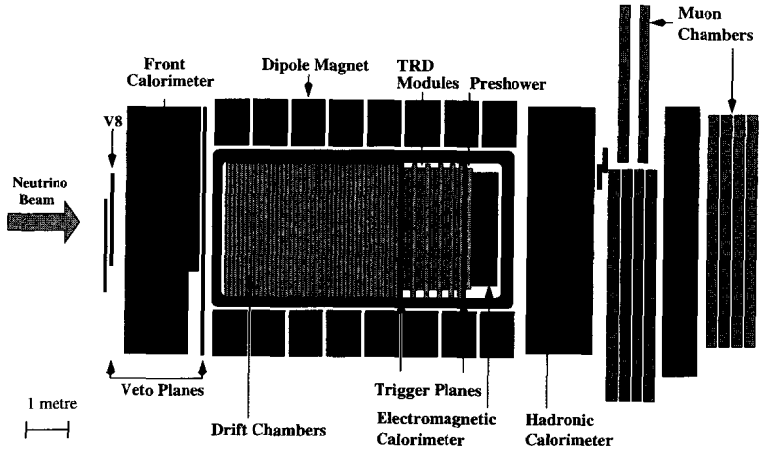

Fig. 3. Side view of the NOMAD detector.

$2.6 \times 2.6 \times 4$ m^3, with an average density of 0.1 g/cm^3. Each chamber contributes only 2% of a radiation length.

Each drift chamber consists of three wire planes with wires at $0°$, $+5°$, and $-5°$ with respect to the magnetic field direction. The spatial resolution for tracks at normal incidence on the chambers is about 150 μm. The resulting momentum resolution, which is a function of both momentum p and length L of the tracks, can be parameterized as:

$$\frac{\sigma_p}{p} \approx \frac{0.05}{\sqrt{L}} \oplus \frac{0.008p}{\sqrt{L^5}}.$$

For momenta less than 10 GeV/c the resolution is $\simeq 3.5\%$, where the dominant contribution comes from multiple scattering.

The drift chambers are followed by a transition radiation detector for electron identification. A set of nine modules, each consisting of a radiator of polypropylene foils followed by a plane of proportional straw tubes filled with a Xe–CH_4 mixture, gives a pion rejection factor greater than 10^3 for a 90% electron efficiency in a momentum range from 1 to 50 GeV/c. Five additional drift chambers are interleaved with the transition radiation modules to provide a precise track extrapolation from the drift chamber target to the following detectors, a preshower and an electromagnetic calorimeter.

The preshower, made of two planes of proportional tubes preceded by a lead plane of 1.6 radiation lengths, is followed by an electromagnetic calorimeter consisting of a matrix of 875 lead-glass Cherenkov counters. The energy resolution for electrons has been measured to be:

$$\frac{\sigma_E}{E} \approx \frac{3.2\%}{\sqrt{E(GeV)}} \oplus 1\%.$$

A hadron calorimeter, consisting of an iron-scintillator sampling calorimeter positioned behind the magnet, is intended to detect neutral hadrons and helps in distinguishing between muons and charged hadrons.

A set of ten drift chambers, each with an active area of 3.75×5.55 m^2 with two planes of drift tubes in the horizontal and two in the vertical directions, are arranged in two muon stations. The first, placed behind the hadron calorimeter, is followed by an 80 cm thick iron absorber and then by the second muon station. The muon momentum thresholds to reach the muon chambers (with 50% probability) are measured to be 2.3 GeV/c for the first muon station and 3.7 GeV/c for the second. The geometrical acceptance for muons to hit either one of the two muon stations is about 98%.

A ν_e CC candidate event detected in NOMAD is shown in Fig. 4. The track pointing to the large cluster in the electromagnetic calorimeter has been identified as an electron. An e^+e^- pair from the conversion of a bremsstrahlung photon emitted by the electron is also present.

3 Search for $\nu_\mu \rightarrow \nu_\tau$ Oscillations

The NOMAD experiment is conducting an appearance search for $\nu_\mu \rightarrow \nu_\tau$ oscillations, which is based on the identification of the τ lepton produced in ν_τ CC interactions. Differently from the CHORUS experiment,[7] where the τ identification is based on the decay topology directly observed in nuclear emulsions, in NOMAD the discrimination of the τ signal against the background of ν_e (ν_μ) CC and ν neutral current (NC) interactions relies on kinematical criteria.

The τ decay products are generally well isolated with respect to the hadronic jet. This can be expressed quantitatively by introducing the variable Q_T, defined as the component of the momentum of visible τ decay products, perpendicular to the total visible momentum vector of the event. Neutral current background, where a particle belonging to the hadronic jet is erroneously taken as coming from a τ decay, is characterized by small values of Q_T, while τ decays have larger Q_T values (see Fig. 5).

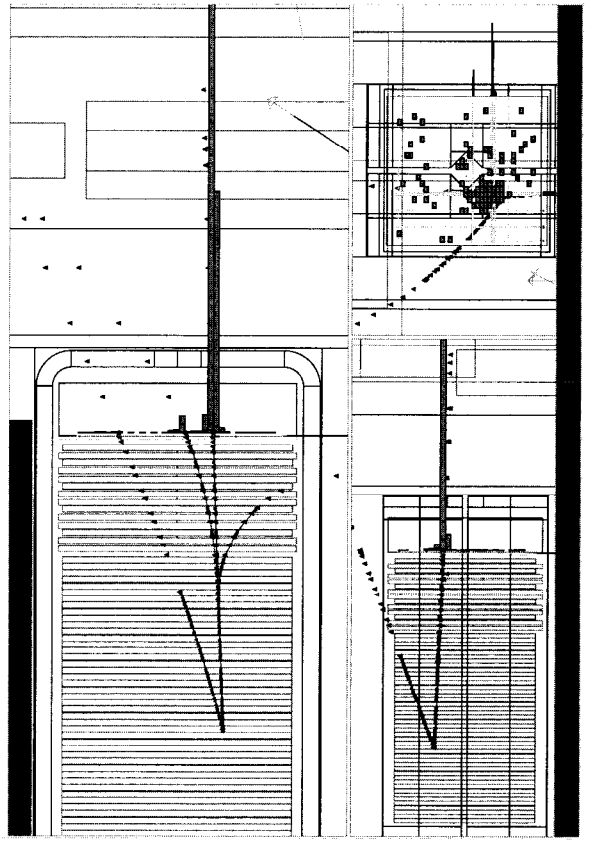

Fig. 4. A ν_e charged current event reconstructed in NOMAD. The longitudinal view orthogonal to the magnetic field is shown on the left. On the right side, the other longitudinal view is represented at the bottom and the transverse view at the top.

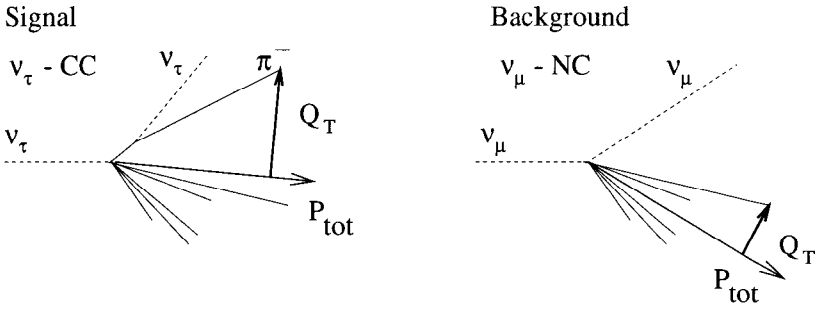

Fig. 5. Visualization of the Q_T variable for the ν_τ-CC signal (on the left), where the produced τ decays to $\tau^- \rightarrow \pi^-\nu_\tau$ and for the ν_μ-NC background (on the right).

The main feature of τ decays is that at least one neutrino carrying away some momentum is present. It is not possible to apply a detailed momentum balance along the neutrino beam direction on an event by event basis since the incoming neutrino momentum is not known. However in the plane transverse to the neutrino beam, as shown in Fig. 6, large missing transverse momentum $\vec{p}_T$ is expected in τ decays from the escaping neutrino(s).[11] In the case of $\nu_{e,\mu}$ CC background, a smaller missing transverse momentum is present due to measurement errors, losses of neutral hadronic particles, and nuclear effects (Fermi motion and nuclear reinteractions). The amount of missing transverse momentum, the angle ϕ_{mh} between $\vec{p}_T$ and the transverse momentum of the hadronic jet $\vec{p}_T^{\,h}$, and the angle ϕ_{lh} between the transverse momentum of the lepton $\vec{p}_T^{\,l}$ and $\vec{p}_T^{\,h}$, completely characterize the kinematics in the transverse plane. The angle ϕ_{mh} is generally larger in ν_τ CC interaction than in $\nu_{\mu,e}$ CC background, where it is almost uniformly distributed. On the other hand, the angle ϕ_{lh} is normally larger for $\nu_{\mu,e}$ background than for the ν_τ signal. Another variable which is useful to characterize the transverse plane kinematics is the transverse mass $M_T = \sqrt{(\mid \vec{p}_T \mid + \mid \vec{p}_T^{\,l} \mid)^2 - (\vec{p}_T^{\,h})^2}$, which is generally large for the neutral current background while it cannot exceed the τ mass in the case of τ decays.

These and many other variables can be used to separate the signal from the background. Each variable X_i provides only some degree of separation. The analysis can be optimized by building probability density functions L for the signal and the back-

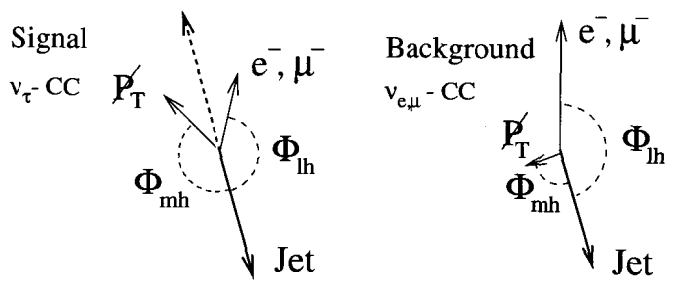

Fig. 6. Kinematical configuration in the transverse plane for ν_τ-CC (on the left), where the produced τ (dashed arrow) decays to electron or muon, and for $\nu_{e,\mu}$-CC interactions (on the right).

ground, approximated by the product of the probability density functions $P(X_i)$ of the set $X_{i=1,N}$ of variables used:

$$L = \prod_{i=1}^{N} P(X_i),$$

where $P(X_i)$ can be one or n-dimensional probability density functions. The likelihood ratio L_R defined as

$$L_R = \frac{L_{Signal}}{L_{Background}}$$

is then used to discriminate signal against background.

In order to avoid biases, the NOMAD collaboration has chosen to conduct a "blind analysis." First of all a comfortably large τ signal region is defined. The analysis procedure is adjusted on the Monte Carlo simulations and by examining the data events outside the signal region. Once reliable estimates of the background and of the signal efficiency have been reached, the analysis cuts are frozen and the events inside the signal region are looked at.

Detectable decays are the electron channel $\tau^- \to e^-\nu_\tau\overline{\nu}_e$, the one-prong hadronic channel $\tau^- \to h^-(+n\pi^0)\nu_\tau$, and the three-prong hadronic channel $\tau^- \to \pi^-\,\pi^-\,\pi^+\nu_\tau$, which have branching ratios of 17.8%, 49.5%, and 10.0%, respectively, thus covering a large part of the possible τ decays. The $\tau \to e$ channel is particularly favored because of the low contamination of ν_e in the beam and its energy spectrum shifted to higher energies with respect to the ν_μ component. The $\tau \to \mu$ channel is not included in the oscillation search because, as will be shown in the following, it is not possible to make a reliable estimate of the background in this case.

The searches in the $\tau^- \to e^-\nu_\tau\overline{\nu}_e$ and $\tau^- \to h^-(+n\pi^0)\nu_\tau$ decay channels will be described here in some detail. These analyses are based on the data collected from 1995 to 1997, as summarized in Table 2.

Table 2. Data sample collected in the years 1995–1997.

Year	ν_μ CC
'95	180,000
'96	380,000
'97	380,000
Total	940,000

3.1 The $\tau^- \to e^-\nu_\tau\overline{\nu}_e$ Channel

The search in the $\tau \to e$ channel begins with the selection of events with only one electron and no muons coming from the primary vertex. The electron, identified as such by the transition radiation detector, the preshower, and the electromagnetic calorimeter, is required to have the first hit of its track at a distance of at most 15 cm from the primary vertex position. A further rejection of electrons coming from photon conversions is achieved by requiring that the invariant mass between the e^- candidate and any positive track from the primary vertex be larger than 50 MeV.

The energy of the electron is carefully reconstructed by taking into account the energy released in the electromagnetic calorimeter and the conversions of bremsstrahlung photons in the drift chamber volume. Electrons with energies larger than 1.5 GeV are accepted as candidates.

Two different likelihood ratios, $L(\tau/CC)$ and $L(\tau/NC)$ (see Fig. 7), have been constructed to reject ν_e CC and ν NC backgrounds, respectively, along the criteria discussed in the previous section.

The likelihood ratio $L(\tau/NC)$ is mainly an estimate of the isolation of the electron candidate from the hadronic jet. It has been built with multi-dimensional probability density functions which make use of the following variables: Q_T and M_T, already defined; the minimum angle between the electron and any track of the hadronic system;

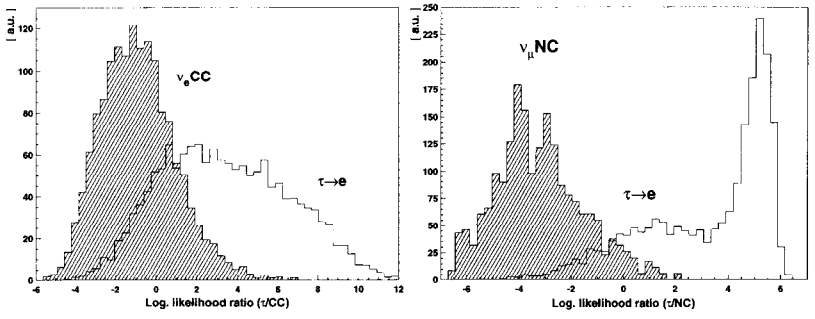

Fig. 7. The logarithm of the likelihood ratios $L(\tau/CC)$ (on the left) and $L(\tau/NC)$ (on the right) for the signal (solid line) and for the background (hatched area).

the angle $\theta_{\nu T}$ between the incident ν direction and the total visible momentum in the event; the angle between the incident ν direction and the total hadron momentum; the electron energy.

The likelihood ratio $L(\tau/CC)$, mainly related to the momentum imbalance in the transverse plane, has been built as a product of two three-dimensional probability density functions, symbolically denoted as:

$$L(\tau/CC) = [p_T^l, p_T^h, \phi_{lh}][E_T, \theta_{\nu T}, Q_{lep}],$$

where, in addition to variables already defined, E_T is the total visible energy and Q_{lep} is the component of the electron momentum perpendicular to the hadronic jet momentum.

The discrimination capability of the $\tau \rightarrow e$ signal against the ν_e CC background, fully expressed by the likelihood ratio $L(\tau/CC)$, can be understood from the inspection of the two-dimensional distributions of the variables which enter in the definition of $L(\tau/CC)$, as shown in Fig. 8.

The $\tau \rightarrow e$ events are both momentum imbalanced and characterized by an electron isolated from the hadronic jet. In a plot of $L(\tau/CC)$ versus $L(\tau/NC)$ (see Fig. 9) the $\tau \rightarrow e$ signal largely lies in the upper right corner, with the background somewhat spread along the diagonal. The thick lines in the upper right part of the plots define the $\tau \rightarrow e$ signal region.

A correct estimate of the background in the signal region cannot rely completely on the Monte Carlo simulation, which critically depends on the correct treatment of the hadronic system. For example, phenomena like nuclear reinteractions, which are

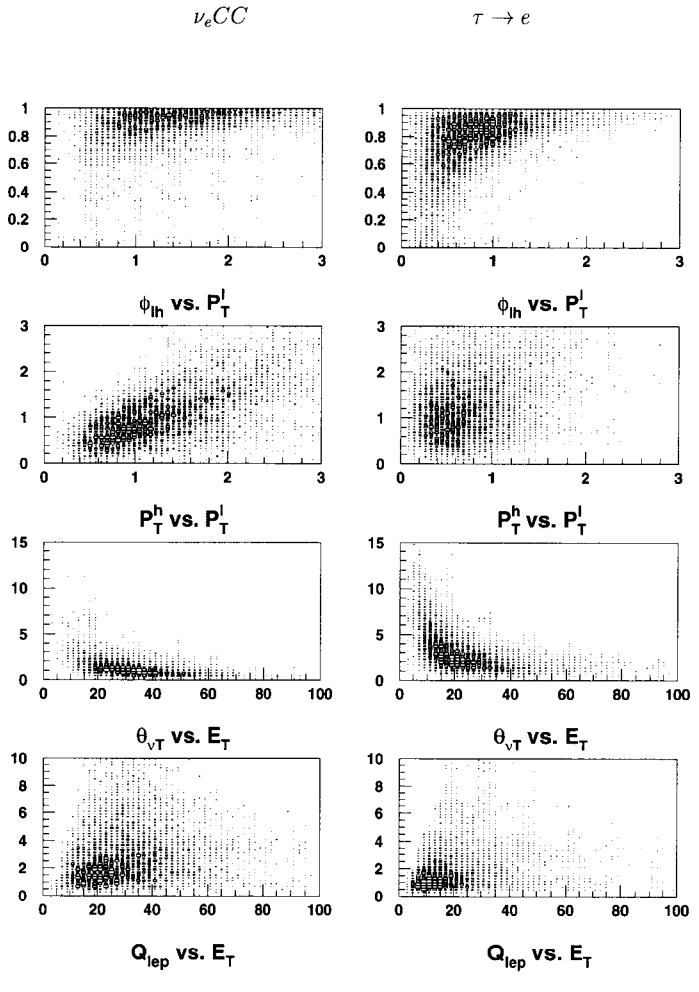

Fig. 8. Two-dimensional plots between the variables which enter in the definition of the likelihood ratio $L(\tau/CC)$, for the case of ν_eCC background (on the left) and for the $\tau \rightarrow e$ signal (on the right).

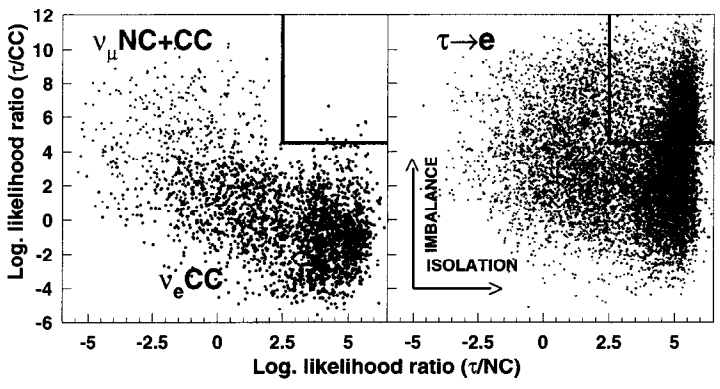

Fig. 9. Plot of $L(\tau/CC)$ versus $L(\tau/NC)$ for the background (on the left) and for the $\tau \rightarrow e$ signal (on the right).

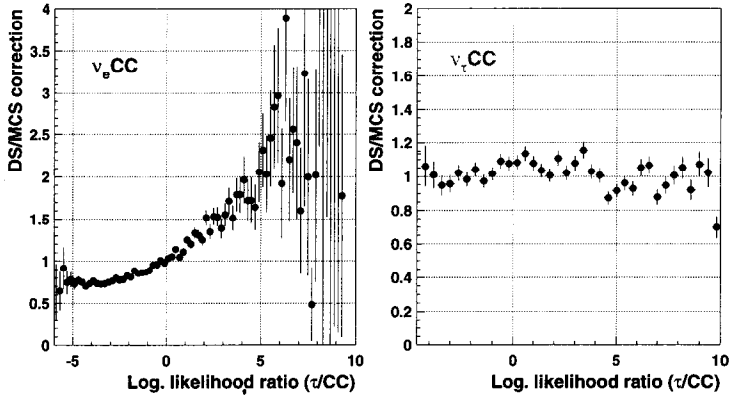

Fig. 10. DS/MCS corrections as a function of the logarithm of $L(\tau/CC)$ for the ν_eCC background (on the left) and for the ν_τCC signal (on the right).

hard to simulate, might affect the kinematics in the transverse plane. For this reason a "data simulator" procedure has been set up, where the data themselves have been used to correct the Monte Carlo estimates of signal efficiencies and background survival fractions. Starting from a measured ν_μ CC event, the identified muon is removed and replaced by another lepton, that is a τ, an electron, or a neutrino, thus getting a "data simulator" (DS) ν_τ CC, a ν_e CC, or a ν NC event, respectively. A similar procedure is applied to Monte Carlo ν_μ CC events in order to produce "Monte Carlo simulator" (MCS) events. DS and MCS events are processed through the same analysis chain as data and Monte Carlo events. Signal efficiencies and background survival fractions (here generically indicated by ϵ) are then obtained through the relation:

$$\epsilon = \epsilon_{MC} \times \frac{\epsilon_{DS}}{\epsilon_{MCS}}$$

where ϵ_{MC} is the Monte Carlo estimate without any "data simulator" correction. The corrections $\epsilon_{DS}/\epsilon_{MCS}$ in the case of ν_e CC background and ν_τ CC signal are shown in Fig. 10 as a function of $L(\tau/CC)$. While the correction is around unity for the ν_τ CC signal, in the case of ν_e CC background, it becomes quantitatively important in the signal region. Since it is not possible to compute data simulator corrections for $\tau \rightarrow \mu$, this channel is not included in the $\nu_\mu \rightarrow \nu_\tau$ oscillation search.

In order to optimize the analysis, a "signal box", where a possible τ signal may be visible, is carefully chosen by studying the sensitivity. This is "defined as the average upper limit one would get from an ensemble of experiments with the expected background and no true signal."[12] The computed sensitivity is shown in Fig. 11 as a function of the lower cut on the likelihood ratio $L(\tau/CC)$. The cut defining the "signal box" is set at the minimum of the sensitivity curve. The rapid increase of the sensitivity observed on the right side of Fig. 11 is due to a loss of signal efficiency in a region where the background is already negligible. Three different likelihood ratio cuts are shown in Fig. 11, the first to indicate the position of the full "signal box" and the other two to show its subdivisions into three different bins. Data events and background estimates are then compared in each of the bins in order to estimate the oscillation probability.

From a similar study on the sensitivity as a function of $L(\tau/NC)$, the full "signal box" is then defined by $L(\tau/NC) > 2.5$ and $L(\tau/CC) > 4.5$. Background estimates and signal efficiency in the "signal box" are shown in Table 3 after "data simulator" corrections. The number N_τ of expected signal events for unit $\nu_\mu \rightarrow \nu_\tau$ oscillation

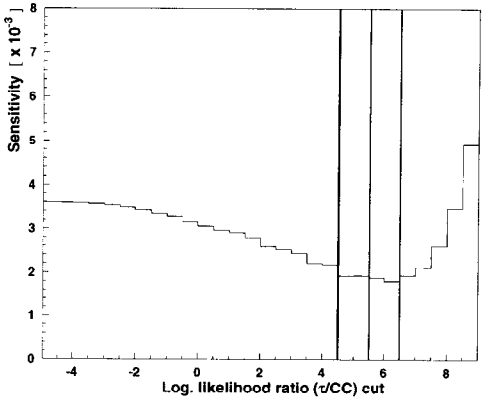

Fig. 11. Sensitivity as a function of the cut on the likelihood ratio $L(\tau/CC)$. The thick vertical line on the left indicates the position of the "signal box" and the other two lines its subdivision into three bins.

Table 3. Background estimates, signal efficiency and N_τ in the "signal box."

Background and efficiencies DS corrected			
ν NC + ν_μ CC backg.	ν_e CC backg.	$\epsilon_\tau(\%)$	N_τ
$0^{+0.4}$	6.6 ± 0.8	4.1 ± 0.3	2904

probability is also shown. N_τ is given by

$$N_\tau = N_\mu \times (\sigma_\tau/\sigma_\mu) \times Br \times \epsilon_\tau,$$

where σ_τ/σ_μ is the suppression factor of the ν_τ cross section (calculated to be 0.48), Br is the decay branching ratio of the $\tau \rightarrow e$ channel, and ϵ_τ is the corresponding τ selection efficiency.

The agreement between data and Monte Carlo predictions after "data simulator" corrections is checked on the electron data outside the "signal box" and on the positron sample (performing a τ^+ search, where no signal is expected in NOMAD). The results are shown in Fig. 12 as a function of the cut on the likelihood ratio $L(\tau/CC)$.

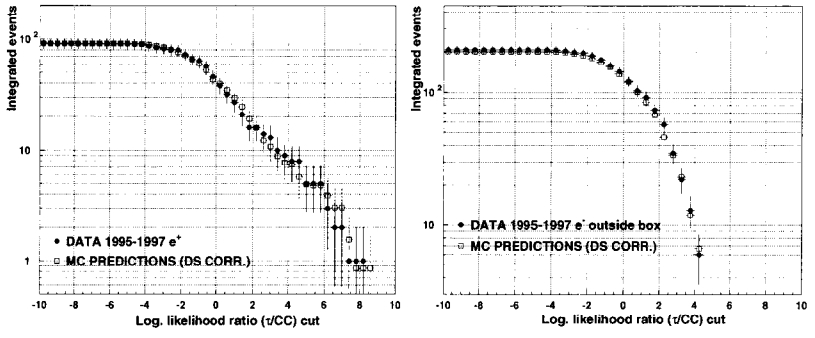

Fig. 12. Number of events surviving in the data (black dots) and corresponding Monte Carlo predictions (white squares) as a function of the cut on the likelihood ratio $L(\tau/CC)$, for e^+ data (on the left) and for e^- data outside the "signal box" (on the right).

Given the quite satisfactory agreement between data and Monte Carlo in Fig. 12, it is allowed to open the "signal box." The results are shown in Fig. 13. Five events are found in the box, with an expected background of 6.6 ± 0.8 events, showing no evidence for oscillations. The table on the right side of Fig. 13 exhibits a good agreement between data events and expected background in each of the bins into which the "signal box" has been subdivided. A final comparison of the likelihood ratio $L(\tau/CC)$ for the estimated background and the data is shown in Fig. 14, where the data follows the background distribution quite satisfactorily.

3.2 The $\tau^- \rightarrow h^-(+n\pi^0)\nu_\tau$ Channel

This decay channel requires the selection of events with no identified muon or primary electron. In addition, events with negative primary tracks with large transverse momentum ($p_T > 0.8$ GeV/c) pointing outside the acceptance of the lepton detectors (muon chambers and electromagnetic calorimeter) are rejected in order to veto charged current events where the lepton cannot be identified. The τ decay candidate is selected as the negative hadron with the highest or second highest p_T in the event.

The rejection of neutral and charged current background events is first accomplished by preliminary cuts on the transverse mass ($M_T < 4$ GeV) and the transverse momentum of the hadronic jet ($p_T^h > 1.3$ GeV/c). As shown in Fig. 15, each of the variables

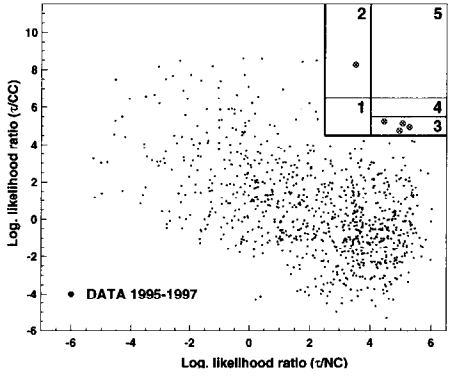

Bin	N_τ	Exp. Backg.	Data
1	240	1.52 ± 0.38	0
2	273	0.23 ± 0.16	1
3	646	3.10 ± 0.57	4
4	543	1.31 ± 0.40	0
5	1202	0.46 ± 0.27	0
Tot.	2904	6.6 ± 0.8	5

Fig. 13. Data distribution in the $L(\tau/NC)$–$L(\tau/CC)$ plane. In the upper right part of the plot the "signal box" with its subdivisions is shown. Data points inside the "signal box" are indicated with large dots. The table on the right side shows data events, expected background, and N_τ in each bin of the "signal box" in the case of $\tau^- \to e^- \nu_\tau \overline{\nu}_e$.

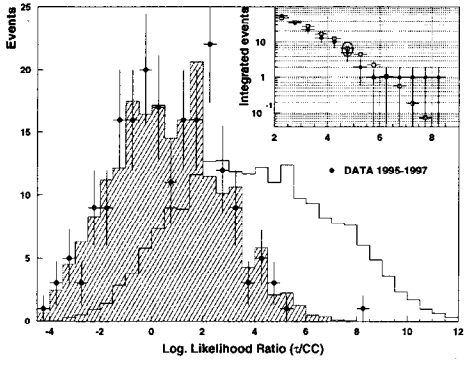

Fig. 14. Logarithm of the likelihood ratio $L(\tau/CC)$ for the data (black dots), estimated background (hatched area), and $\tau \to e$ signal (solid line). The inset shows the number of events surviving in the data (black dots) and the corresponding Monte Carlo predictions (white squares) as a function of the cut on $L(\tau/CC)$.

Q_T, the transverse mass M_T, and $\rho_m = \mid \vec{p}_T \mid / (\mid \vec{p}_T^{\,\pi} \mid + \mid \vec{p}_T^{\,h} \mid + \mid \vec{p}_T \mid)$ can achieve some isolation of the τ signal from the neutral and charged current background events. By making use of these quantities, a likelihood ratio is built (see Fig. 15) according to

$$L = ([Q_T, M_T, \rho_m], \frac{p^\pi}{E_{vis}}, p_T^h).$$

This is the product of the three-dimensional probability density function of the variables Q_T, M_T, and ρ_m with the one-dimensional probability density functions of the variables p_T^h and of the ratio $\frac{p^\pi}{E_{vis}}$ between the hadron candidate momentum and the visible energy.

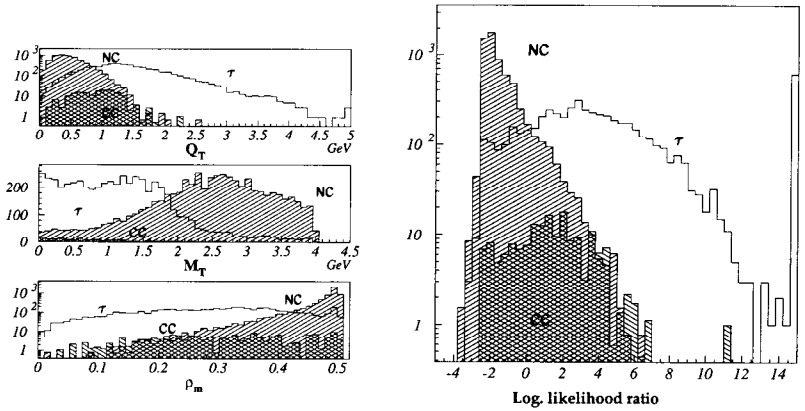

Fig. 15. Distributions of the variables Q_T, M_T, and ρ_m (on the left side), and of the logarithm of the likelihood ratio (on the right side) are shown for the τ signal, CC, and NC background.

The "signal box," defined by the logarithm of the likelihood ratio being larger than seven, is further subdivided into three bins, as shown in Fig. 16. Here the efficiency for $\tau^- \to h^-(+n\pi^0)\nu_\tau$, the background, and the sensitivity are shown as a function of the cut on the likelihood ratio.

The number of data events in the "signal box" is consistent with the expected background, as summarized in Table 4.

4 Present Results

Results from the analysis of the 1995 data have already been published,[13] obtaining a limit on the oscillation probability of $P(\nu_\mu \to \nu_\tau) < 2.1 \times 10^{-3}$ at 90% confidence level.

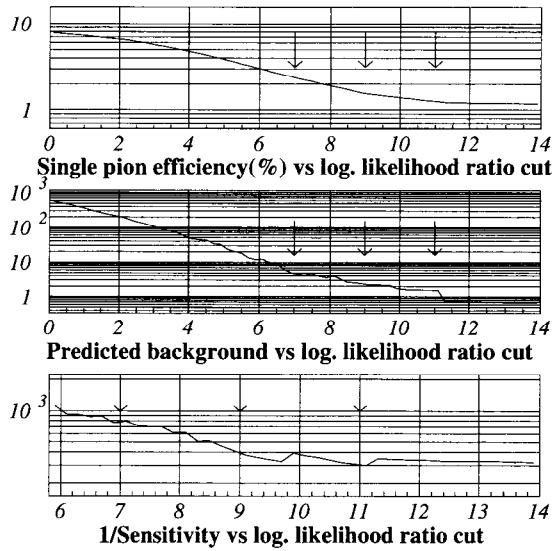

Fig. 16. The single π efficiency, the expected background, and the sensitivity are shown as a function of the likelihood ratio cut. The vertical arrows indicate the cuts defining the "signal box" and its subdivisions.

The present status of the analysis for the different τ decay channels is summarized in Table 5.

For each τ decay channel, two different analyses have been carried out. One, indicated as "DIS," starts from a sample of events with a hadronic jet momentum larger than 1.5 GeV/c, consisting mainly of deep inelastic events. The analyses discussed in the previous section are of this kind. For data events with the total hadron momentum smaller than 1.5 GeV/c, a specific analysis, here indicated as "LM," has been performed. This takes into account the low multiplicity of the hadronic system in this sample of events, which is enriched in quasi-elastic and resonance interactions. The "LM" analysis has not yet been extended to the '96–'97 data.

The expected total background is in good agreement with the number of events observed in the data. Following the statistical procedure based on the unified Feldman-Cousins approach,[12] we can set a limit on the oscillation probability of $P(\nu_\mu \to \nu_\tau) <$ 0.6×10^{-3} at 90% confidence level. The approximate sensitivity of the experiment for the number of expected background events is 0.8×10^{-3}.

From the L/E (traveled distance over energy) distribution of ν_μ neutrinos interacting in NOMAD, an exclusion region in the $\Delta m^2 - \sin^2 2\theta$ plane can be derived as shown in Fig. 17. This gives an upper limit on $\sin^2 2\theta_{\mu\tau}$ at large Δm^2 of 1.2×10^{-3} at 90% confidence level. The CHORUS experiment[7] has obtained a comparable limit. Given the 1% contamination of electron neutrinos in the beam, it is possible to set a limit on the $\nu_e \to \nu_\tau$ oscillation probability. The preliminary upper limit on $\sin^2 2\theta_{e\tau}$ at large Δm^2 is 8×10^{-2} at 90% confidence level.

Table 4. Data events, expected background, and N_τ are shown in each bin of the "signal box" in the case of the $\tau^- \to h^-(+n\pi^0)\nu_\tau$ decay channel.

Likelihood	N_τ	Exp. Backg.	Data
7-9	664	2.3 ± 0.8	3
9-11	234	$1.1^{+0.8}_{-0.6}$	2
> 11	1133	$1.1^{+0.7}_{-0.5}$	0
> 7	2031	4.5 ± 1.2	5

Table 5. Summary of the analyses in the different τ decay channels for deep inelastic and low multiplicity interactions. The data sample used, the expected background, the number of events observed in the data, and N_τ are given for each decay channel.

Channel	Data	Exp. Backg.	N_{obs}	N_τ
$\tau^- \to e^- \nu_\tau \bar{\nu}_e$ DIS	'95–'97	6.6 ± 0.8	5	2904
$\tau^- \to e^- \nu_\tau \bar{\nu}_e$ LM	'95	$0.5^{+0.6}_{-0.2}$	0	218
$\tau^- \to h^-(+n\pi^0)\nu_\tau$ DIS	'95–'97	4.5 ± 1.2	5	2031
$\tau^- \to h^-(+n\pi^0)\nu_\tau$ LM	'95	$0.1^{+0.3}_{-0.1}$	1	198
$\tau^- \to \rho^- \nu_\tau$ DIS	'95–'97	$5^{+1.2}_{-0.9}$	5	1900
$\tau^- \to \pi^- \pi^- \pi^+ \nu_\tau$ DIS	'95–'96	7.0 ± 2.7	5	1011
$\tau^- \to \pi^- \pi^- \pi^+ (+n\pi^0)\nu_\tau$ LM	'95	$0.4^{+0.6}_{-0.4}$	0	108
Total		24.1 ± 3.3	21	8370

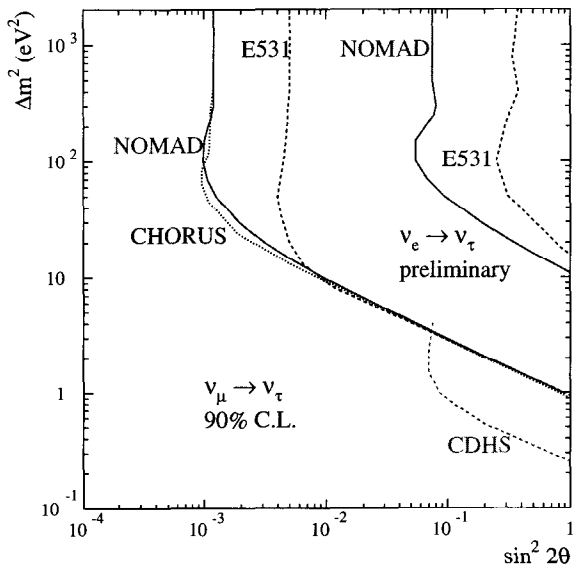

Fig. 17. NOMAD 90% C. L. exclusion plots for $\nu_\mu \rightarrow \nu_\tau$ and $\nu_e \rightarrow \nu_\tau$ oscillations (solid lines). The results of the CHORUS experiment[7] (dotted line) and of the previous E531 experiment[14,2] (dashed lines) using the technique of nuclear emulsions are shown.

5 Conclusions

NOMAD has set an upper limit on the $\nu_\mu \rightarrow \nu_\tau$ oscillation probability of 0.6×10^{-3} at 90% confidence level. The result has been achieved from the analysis of about 9.4×10^5 charged current interactions collected in the years from 1995 to 1997. The presence of a τ signal has been searched for in a large fraction of the possible τ decay channels. The quality of the event reconstruction which is currently being improved, the additional data collected in 1998, and the extension of all the analyses to the full available data sample will provide further sensitivity in the near future.

References

[1] E. D. Commins and P. H. Bucksbaum, *Weak Interactions of Leptons and Quarks* (Cambridge University Press, Cambridge, 1983); L. B. Okun, *Leptons and Quarks* (North-Holland, Amsterdam, 1982).

[2] Particle Data Group, C. Caso *et al.*, Eur. Phys. J. C **3**, 1 (1998).

[3] S. M. Bilenky and B. Pontecorvo, Phys. Rev. **4**, 225 (1978) and references therein.

[4] J. M. Conrad, to be published in *Proceedings of the* 29^{th} *International Conference on High-Energy Physics (ICHEP 98),* (Vancouver, Canada, July 1998); see also hep-ex/9811009; M. Nakahata, "Results from SuperKamiokande," these proceedings; G. Mills, "Results from LSND," these proceedings.

[5] NOMAD Collaboration, P. Astier *et al.*, CERN-SPSLC/91-21 (1991); Addendum 1, CERN-SPSLC/91-48 (1991); Addendum 2, CERN-SPSLC/91-53 (1991).

[6] NOMAD Collaboration, J. Altegoer *et al.*, Nucl. Instrum. Methods A **404**, 96 (1998).

[7] CHORUS Collaboration, E. Eskut *et al.*, Phys. Lett. B **424**, 202 (1998); CHORUS Collaboration, E. Eskut *et al.*, Phys. Lett. B **434**, 205 (1998); G. Catanesi, "Results from CHORUS," these proceedings.

[8] H. Harari, Phys. Lett. B **216**, 413 (1989).

[9] G. Acquistapace *et al.*, CERN-ECP/95-14 (July 1995).

[10] B. Van de Vyver, Nucl. Instrum. Methods A **385**, 91 (1997); M. C. Gonzalez-Garcia and J. J. Gomez-Cadenas, Phys. Rev. D **55**, 1297 (1997).

[11] C. H. Albright and R. E. Shrock, Phys. Lett. B **84**, 123 (1979); C. H. Albright, R. E. Shrock, and J. Smith, Phys. Rev. D **20**, 2177 (1979).

[12] G. J. Feldman and R. D. Cousins, Phys. Rev. D **57**, 3873 (1998).

[13] NOMAD Collaboration, J. Altegoer *et al.*, Phys. Lett. B **431**, 219 (1998).

[14] E531 Collaboration, N. Ushida *et al.*, Phys. Rev. Lett. **57**, 2897 (1986).